Dynamic stresses in an elastic half-space

Citation: Schepers, Winfried, Stavros Savidis, and Eduardo Kausel. "Dynamic Stresses in an Elastic Half-Space." Soil Dynamics and Earthquake Engineering 30, no. 9 (September 2010): 833–843.

As Published: http://dx.doi.org/10.1016/j.soildyn.2009.11.004

Publisher: Elsevier

Persistent URL: http://hdl.handle.net/1721.1/101653

Version: Author's final manuscript: final author's manuscript post peer review, without publisher's formatting or copy editing

Soil Dynamics and Earthquake Engineering 30 (2010) 833–843

Dynamic Stresses in an Elastic Half-space

by

Winfried Schepers[1]
Stavros Savidis[2]
Eduardo Kausel[3]

Hommage à Prof. Anestis Veletsos

Abstract

This paper deals with the problem of time-varying point loads applied onto the surface of an elastic half-space and the stresses that such loads elicit within that medium. The emphasis is on the evaluation of the isobaric contours for all six of the stress components at various frequencies of engineering interest and for a full range of Poisson's ratios. The extensive set of pressure bulbs presented herein may of help in predicting the severity of dynamic effects in common practical situations in engineering —or even the lack thereof.

Introduction

Perhaps few problems are more familiar to geotechnical engineers than the assessment of settlements caused by loads applied onto the surface of a soil, and part of such task relies on estimating the excess stresses elicited within the soil mass by the applied load. The latter are often obtained by assuming the soil to be relatively homogeneous, and inferring the stresses at depth from normalized nomographs for either circular or square vertical and horizontal loads applied on the surface in the context of a superposition scheme to obtain the stresses for arbitrarily loaded areas. Alternatively, the exact formulae for the so-called Boussinesq and Cerruti problems can also be used to directly determine the desired stresses, provided that the points in the soil where the stresses are sought lie deeper than the characteristic dimensions of the foundation so that only the intensity and not the spatial distribution of the load is relevant. The aim of this paper is to extend this technique to dynamic loads applied on the surface with a harmonic variation in time.

Pressure Bulb for Static Loads

Intimately related to the problem of stresses in the ground is the concept of the *pressure bulb*, which is simply a contour plot of the stress components with depth. Considering that the homogeneous elastic half-space is a medium lacking any characteristic length, the stress components anywhere do *not* depend on the elastic moduli, although they generally depend on Poisson's ratio ν, or alternatively, on the ratio of the elastic Young modulus to the shear modulus, $E/G = 2(1+\nu)$.

It is a rather remarkable fact that in the ideal case of a homogeneous elastic half-space subjected to *static* point loads in any direction applied at the surface, the stresses in horizontal planes do *not*

[1] Doctoral candidate and graduate research assistant, Berlin Institute of Technology (see address below)
[2] Professor and Chair of Soil Mechanics and Geotechnical Engineering, Berlin Institute of Technology, TIB1-B7, Gustav-Meyer-Allee 25, 13355, Berlin, Germany
[3] Professor of Civil and Environmental Engineering, Massachusetts Institute of Technology, Cambridge, MA 02139

depend on Poisson's ratio (see Appendix I for a full list of these stresses). Inasmuch as the stresses in the soil due to an arbitrary static load distribution on the surface —including the contact stresses elicited by a rigid foundation welded to the soil and undergoing any mode of displacement, including rocking— are obtained by simple superposition of (i.e. convolution with) the stresses due to a point load, it is clear that such stresses must be independent of Poisson's ratio as well, even if the rigidity of the plate should depend on that ratio. Inasmuch as the spatial distribution of contact stresses underneath a smooth rigid plate does not depend on Poisson's ratio, this means that for any total horizontal-vertical load applied to the plate, the stresses in horizontal planes will not change either as this ratio varies continuously from $\nu = 0$ to $\nu = 0.5$. Peculiarly, this property does not hold for any of the displacement components, which depend all on Poisson's ratio, and stranger still, this privileged property of the half-space does *not* extend to the full space either, even though it is more "regular" and "simpler", and thus could be expected to exhibit further symmetries. We hasten to add, however, that this remarkable property ceases to hold when the soil is inhomogeneous and/or consist of two or more layers, or the load is not on the surface, or the loads are dynamic as considered herein.

With reference to the coordinate system and definitions shown in Figure 1 and the formulas listed in Appendix 1, it follows that the static stresses in an elastic half-space are inversely proportional to the square of the distance to the load. Choosing an arbitrary reference distance R_0, a reference inclination ϕ_0 (either $0^\circ, 45^\circ$ or 90° depending on both the stress component and the load case), and a reference azimuth $\theta_0 = 0^\circ, 90^\circ$ as they case may require, we can divide that stress by its value at the reference location, i.e.

$$\frac{\sigma_{ij}}{\sigma_{ij}^0} = \left(\frac{R_0}{R}\right)^2 f_{ij}\left(\phi, \phi_0, \nu\right) \tag{1}$$

Setting this ratio to ± 1 for equal stress amplitudes and solving for the radial distance, we obtain

$$\frac{R}{R_0} = \sqrt{\left| f_{ij}\left(\phi, \phi_0, \nu\right)\right|} \tag{2}$$

The locus defined by this equation is referred to as the *pressure bulb* for that stress component. For a horizontal load, it changes as $\cos\theta$ or $\sin\theta$ around the vertical axis, and it is rotationally symmetric for vertical loads. Clearly, this function equals unity at $\phi = \phi_0$, at which $R / R_0 = 1$. In general, this function is defined everywhere, except at the point of application of the load $R = 0$, where a singularity will be observed. Surfaces of other equal stress magnitudes are homothetic[4] to the reference pressure bulbs defined by the equation above, and their magnitudes are inversely proportional to the square of their linear size, that is, $\sigma_{ij}\left(R\right) = \left(R_0 / R\right)^2 \sigma_{ij}\left(R_0\right)$. Except for the radial component that depends explicitly on Poisson's ratio, all other ratios are independent of this ratio, because the factor in ν cancels out in all cases except for σ_r. This means that the shape of most static pressure bulbs do not depend on Poisson's ratio. These static pressure bulbs are

[4] Homothecy: Enlargement (or contraction) of a figure relative to some arbitrary center from which all radial lines are increased by the same factor. This transformation changes the size, but not the shape of the figure.

shown later on as special cases of the dynamic pressure bulbs, where it should be observed that the presence of multiple lobes in any one quadrant of a pressure bulb is an indication of stress reversals.

We comment in passing about another remarkable characteristic of the solution to the Cerruti problem (i.e. the horizontal point load problem), namely that the tangential shearing stress in horizontal planes $\tau_{\theta z}$ (which equals the vertical shearing stress $\tau_{z\theta}$ in vertical-radial planes) vanishes everywhere, i.e. $\tau_{\theta z} = 0$. This will not be the case for the dynamic stress, which means that the concept of dynamic magnification for that stress component is meaningless, inasmuch as the magnification factor would be infinite everywhere.

Displacements and stresses due to harmonic loads

A very general method to obtain the displacement field caused by a load distribution on the surface having a harmonic (or static) variation in time is by means of integral transforms. The details are well-known, so only final results need be shown, and even these can be relegated to Appendix II. The interested reader may find full derivations in Chapter 10 of Kausel (2006), among other sources. For circular loads of radius a, such integral (i.e. *Hankel* or Fourier-Bessel) transforms are of the form

$$I_{mn} = \int_0^\infty f\left(\omega, k, r, z\right) J_m\left(kr\right) J_n\left(ka\right)\, dk \tag{3}$$

in which ω is the frequency of excitation, k is the horizontal wavenumber, r, z is the range and depth (i.e. position) of the receiver in cylindrical coordinates, $m, n = 0,1$ are indices that depend on the load case and response direction being considered, and J_m, J_n are Bessel functions of the first kind and order m, n as the case may be. Also, $f\left(\omega, k, r, z\right)$ is an appropriate flexibility function (or Green's function), which depends on the frequency and the horizontal wavenumber. Additional details can be found in Appendix II.

In principle, a formulation based on integral transforms is exact, but in only rare cases are such improper integrals tractable by exact analytical means, e.g. Veletsos & Wei (1971). In fact, even in the static case and when the loads are distributed rather than concentrated, closed-form expressions are generally lacking, even if they are known for some loads distributions. Thus, the integrals must be evaluated numerically, a task that is fraught with difficulties. Among the problems encountered are:

a) The singularity at the so-called Rayleigh pole;
b) The rapid oscillation of the kernels (integrands) when either the range r or the frequency ω is large; and
c) The contribution of the tail beyond which the numerical integrals must necessarily be truncated. While the kernel is oscillatory, it decays roughly as k^{-1} for receivers at the same elevation as the source, so the contribution of the tail is not negligible.

An excellent strategy to deal with the latter problem is to subtract the static solution in the wavenumber domain from the kernel, and then add it back in the spatial domain, considering that it is known in closed form, at least for point loads. That way, the tail virtually disappears.

Clearly, an integral transform solution is strictly *numerical*, even if the underlying formulation should be exact.

After carrying out the integral transforms, the displacements in the soil are found to be of the form

$$u(\omega,r,\theta,z)=U(\omega,r,z)\begin{pmatrix}\cos n\theta\\ \sin n\theta\end{pmatrix} \tag{4}$$

in which the choice of trigonometric function depends on the direction of both the load and of the response, and $n=0,1$ for vertical and horizontal loads, respectively. Also, $U(\omega,r,z)$ is a response function which is generally complex, so it has both amplitude and phase. Similar expressions can be written for the other components, and any of these can readily be evaluated over some appropriately fine grid and plotted as may be needed.

The solution being numerical, the final displacements are known only at points on a grid, and not as functions over the continuum. Thus, a direct evaluation of the strains from the displacements would in principle call for the use of finite differences. To avoid this problem, it is preferable to formulate the strains and stresses directly in the frequency-wavenumber domain and obtain their values by numerical integration over wavenumbers, and this is precisely the strategy pursued in this work. At least for point loads on the surface, the static components of the stresses in the wavenumber domain can be subtracted from the kernels, and later on, their contribution added back in the spatial domain, as described in Appendix II.

Dynamic Pressure Bulb

To illustrate the differences between static and dynamic stresses and begin to focus ideas, we proceed to make a brief detour and consider first the case of a dynamic vertical point load acting within a *full*, homogeneous space, i.e. the so-called Stokes problem. In comparison to the half-space, this problem has the advantage that its solution is known in closed form throughout, both in the time domain and in the frequency domain; thus its usefulness as a fundamental solution in the Boundary Element Method. Hence, we can use this solution to help us surmise the general form of the solution for the half-space. The vertical stress due to a harmonic vertical point load in a full space can be shown to be given by (Kausel, 2006):

$$\sigma_z=\frac{\gamma_3}{4\pi R^2}\left\{2\left[\left(R\frac{\partial\chi}{\partial R}-3\chi\right)\gamma_3^2+R\frac{\partial\psi}{\partial R}+2\chi-\psi\right]+\frac{2\nu}{1-2\nu}\left[R\frac{\partial(\chi+\psi)}{\partial R}+\chi-\psi\right]\right\} \tag{5}$$

with

$$\gamma_3=\frac{z}{R}=-\cos\phi \tag{6a}$$

$$\psi=e^{-\mathrm{i}\Omega_P}\left(\frac{C_S}{C_P}\right)^2\left\{\frac{\mathrm{i}}{\Omega_P}+\frac{1}{\Omega_P^2}\right\}+e^{-\mathrm{i}\Omega_S}\left\{1-\frac{\mathrm{i}}{\Omega_S}-\frac{1}{\Omega_S^2}\right\} \tag{6b}$$

$$\chi = e^{-\mathrm{i}\Omega_P}\left(\frac{C_S}{C_P}\right)^2\left\{1-\frac{3\mathrm{i}}{\Omega_P}-\frac{3}{\Omega_P^2}\right\}-e^{-\mathrm{i}\Omega_S}\left\{1-\frac{3\mathrm{i}}{\Omega_S}-\frac{3}{\Omega_S^2}\right\} \tag{6c}$$

$$R\frac{\partial\psi}{\partial R} = e^{-\mathrm{i}\Omega_P}\left(\frac{C_S}{C_P}\right)^2\left[1-\frac{2\mathrm{i}}{\Omega_P}-\frac{2}{\Omega_P^2}\right]-e^{-\mathrm{i}\Omega_S}\left[1+\mathrm{i}\Omega_S-\frac{2\mathrm{i}}{\Omega_S}-\frac{2}{\Omega_S^2}\right] \tag{6d}$$

$$R\frac{\partial\chi}{\partial R} = e^{-\mathrm{i}\Omega_S}\left[3+\mathrm{i}\Omega_S-\frac{6\mathrm{i}}{\Omega_S}-\frac{6}{\Omega_S^2}\right]-e^{-\mathrm{i}\Omega_P}\left(\frac{C_S}{C_P}\right)^2\left[3+\mathrm{i}\Omega_P-\frac{6\mathrm{i}}{\Omega_P}-\frac{6}{\Omega_P^2}\right] \tag{6e}$$

$$\Omega_S = \frac{\omega R}{C_S}, \qquad \Omega_P = \frac{\omega R}{C_P}, \qquad \frac{1}{\Omega_P} = \frac{1}{\Omega_S}\left(\frac{C_S}{C_P}\right) = \frac{1}{\Omega_S}\sqrt{\frac{1-2\nu}{2(1-\nu)}} \tag{6f}$$

$$\left(\frac{\Omega_P}{\Omega_S}\right)^2 = \left(\frac{C_S}{C_P}\right)^2 = \frac{1-2\nu}{2(1-\nu)} \tag{6g}$$

In the limit of zero frequency (static load), the functions ψ, χ are no longer functions of position, but are constants:

$$\chi = \frac{1}{4(1-\nu)}, \qquad \psi = \frac{3-4\nu}{4(1-\nu)} = 1-\chi, \qquad \frac{\partial\psi}{\partial R} = \frac{\partial\chi}{\partial R} = 0 \tag{7}$$

in which case

$$\sigma_z = -\frac{\gamma_3}{8\pi R^2(1-\nu)}\left(1-2\nu+3\gamma_3^2\right) \tag{8}$$

and

$$\frac{\sigma_z(\Omega_S,\gamma_3)}{\sigma_z(0,\gamma_3)} = -\frac{2(1-\nu)}{1-2\nu+3\gamma_3^2}\left\{2\left[\left(R\frac{\partial\chi}{\partial R}-3\chi\right)\gamma_3^2+R\frac{\partial\psi}{\partial R}+2\chi-\psi\right]+\frac{2\nu}{1-2\nu}\left[R\frac{\partial(\chi+\psi)}{\partial R}+\chi-\psi\right]\right\} \tag{9}$$

As can be seen, the ratio of dynamic to static vertical stress does not depend explicitly on R, because neither ψ, χ nor the products $R\,\partial\chi/\partial R$, $R\,\partial\psi/\partial R$ are functions of R. However, this ratio is not only a complex function of the dimensionless frequency Ω_S, but depends also on the inclination $\gamma_3 = z/R = -\cos\phi$ of the source-receiver line with the vertical axis. Hence, surfaces of constant *static stress* do *not* coincide with surfaces of constant *dynamic stress*. That is, the shape of the pressure bulb evolves with frequency. Furthermore, because the functions involved are complex, the pressure bulb for dynamic loads are generally defined in terms of contours of equal magnitude and phase, both of which form a set of orthogonal lines.

The case of a half-space is similar to that of the full space in that the problem lacks a characteristic length. Hence, the products $\sigma_{ij} R^2$ will solely be functions of the dimensionless frequency Ω_S, of the direction angles ϕ, θ and of Poisson's ratio ν, but not of R. Thus, for any given dimensionless frequency Ω_S, the response functions can be obtained and evaluated over a dense grid in the neighborhood of $R \approx 1$, normalized by the corresponding static stress at the reference location R_0, ϕ_0, and from the resulting magnification field a set of contour lines can be inferred and then plotted in terms of magnitude and phase. The exception is $\tau_{\theta z}$, which does not exist in the static case, and can thus only be plotted by itself without scaling or normalization.

After implementing the formulation succinctly outlined above to the problem of harmonic point loads acting on the surface of an elastic half-space —the so-called Lamb's problem— we have obtained displacements and stresses over a sufficiently large grid in the neighborhood of the load from which contour lines for equal amplitudes that constitute the pressure bulbs were obtained. Figures 2 through 7 show the set of bulbs for all stress components at three different values of Poisson's ratio, namely $\nu = 0,\ 0.33,\ 0.49$. All bulbs were computed with a model for which the nominal shear wave velocity is $\tilde{C}_s = 200$ m/s and the nominal radial distance to the reference point on the static bulb is $R_0(\phi_0) = 1$ meter (i.e. the radial distance along the ray $\phi_0 = 0^\circ, 45^\circ, \text{or} 90^\circ$, depending on the stress component).

To help interpret the results shown in these plots, begin with a thought experiment. Consider for this purpose any given stress component, say σ_z i.e. the vertical stress due to a vertical load. Then for constant Poisson ratio and constant shear wave velocity, this stress (in spherical coordinates) is of the form

$$\sigma_z = \frac{F_z(a_0, \phi)}{R^2} \tag{10}$$

where $a_0 = \omega R / C_s$ is the dimensionless frequency, R is the radial distance, and ϕ is the angle from the vertical. The dynamic bulbs shown in Figs. 2 to 7 have all the same amplitude, so if R_0, R_1 are respectively the radial distances to the static and dynamic contours at some dimensionless frequency a_0, then by definition

$$\frac{F_z(\omega R_1 / C_s,\ \phi)}{R_1^2} = \frac{F_z(0, \phi)}{R_0^2} \tag{11}$$

It follows that

$$\frac{F_z(a_0, \phi)}{R_1^2} = \left(\frac{R_1}{R_0}\right)^2 \frac{F_z(0, \phi)}{R_1^2} \tag{12}$$

or

$$\frac{\sigma_z(a_0, R_1, \psi)}{\sigma_z(0, R_1, \psi)} = \left(\frac{R_1}{R_0}\right)^2 \tag{13}$$

The above expressions imply all of the following:

1) While the frequency ω is constant on each contour, the dimensionless frequency a_0 is not, because the bulbs are not at a constant radial distance from the load, i.e. $R = R(\phi)$. Thus, on any one contour $a_0 = a_0(\phi)$.
2) The dimensionless frequency a_0 depends also on the shear wave velocity C_s, which generally will differ from the nominal $\tilde{C}_s = 200$ m/s used herein. Hence, all frequencies annotated on the contours must be scaled in the ratio $C_s / \tilde{C}_s$ (i.e. softer soils imply lower frequencies, stiffer soils imply higher frequencies).
3) The ratio of dynamic to static stress at any arbitrary point for some stresses observed along the ray ϕ = constant —the dynamic amplification factor—equals the ratio squared of the scaled (i.e. nominal) radial distances to the dynamic and static bulbs, which again depends on the inclination angle ϕ. Hence, the degree of separation of the bulbs is a measure of the severity of dynamic effects due to wave propagation and focusing.
4) All pressure bulbs can be enlarged homothetically with respect to the point of application of the load by any arbitrary factor without affecting their relative shapes. However, because of the dependence of the dimensionless frequency on the radial distance, this implies that the frequencies for each contour line thus augmented in size would drop in proportion to the geometric scaling factor. For example, if the bulbs were enlarged by a factor 10 i.e. $R_0(\phi_0) = 10$ m, then the frequencies of all bulbs would have to be divided by 10.

It should be added that while the static bulbs lack any scale length, strictly speaking the dynamic bulbs do indeed have one, namely the wavelength of shear waves $\lambda = 2\pi C_s / \omega$. Hence, the dimensionless frequency can be interpreted as a measure of the radial distance in wavelengths, i.e.

$$a_0 = \omega R / C_s = 2\pi R / \lambda \tag{14}$$

Thus, homothecy for the dynamic bulbs continues to hold if the radial distance to any bulb, expressed in wavelengths, remains constant. A brief discussion of the implications of the previous considerations is taken up in the next section.

Conclusions

As indicated earlier, all dynamic bulbs were computed using a nominal shear wave velocity of 200 m/s and evaluated in the neighborhood of $R \sim 1$ meter. The following conclusion may be drawn:

- At low to moderate frequencies, say below 25 Hz, the dynamic effects range from negligible to moderate, and can probably be ignored. However, observe that this frequency threshold descends in tandem with the ratio of actual to nominal shear wave velocity, i.e. $C_s / \tilde{C}_s$. Above that threshold, the dynamic effects become very important and stress patterns are evident which deviate substantially from the static. This effect is particularly relevant to the design of machine foundations.

- Dynamic stresses reach deeper into the soil, and strong focusing (directivity) effects become readily apparent. In addition, additional lobes and shadow zones appear which add complexity to the stress patterns. These result from constructive and destructive interference of waves.
- The dynamic stress bulbs depend strongly on Poisson's ratio, and become especially dramatic for nearly incompressible soils ($\nu = 0.49$).
- The stress component $\tau_{\theta z}$, which for none of the two static cases exists, exhibits strong frequency dependence for dynamic horizontal loads.

A word in closing: Sharp-eyed readers may well have noticed that there exist stress bulbs for which the contour lines intersect other lines. This is not an error because the contour lines are for different frequencies, so they have a different physical meaning. The various contour lines only share one common attribute, namely that their amplitude of stress is the same, even if not phase.

[Note: The online version of this paper has all figures in color.]

Acknowledgement:

This paper was written in honor of Prof. Anestis Veletsos —*Andy* to his friends—in tribute of his magnificent and pioneering contributions to earthquake engineering, soil dynamics and soil-structure interaction. May he enjoy many more years of productive achievements.

References

Boussinesq, V.J. (1885): Application des Potentiels a L'Étude de L'Équilibre et du movement des Solides Élastiques, Paris, *Gauthier-Villars*, Imprimeur-Libraire

Cerruti, Valentino (1882): "Ricerche intorno all'equilibrio dei corpi elastici isotropi", *Reale Accademia dei Lincei*, Roma, Vol.13.

Kausel, E. (2006): Fundamental Solutions in Elastodynamics: A Compendium, Cambridge University Press (a brief Corrigendum is available from the author by request).

Poulos, H. G. and Davis, E. H. (1974): Elastic Solutions for Soil and Rock Mechanics, John Wiley.

Veletsos, A.S. and Wei, Y.T. (1971): "Lateral and Rocking Vibration of Footings", *J. Soil. Mech. Found. Div.*, ASCE, 97, 1227-1248

Appendix I: Static stresses in Cerruti and Boussinesq problems

Consider a right-handed system of cylindrical coordinates in which both z and the vertical load are positive up, see Figure 1. Also, $r=\sqrt{x^2+y^2}$ is the range, $R=\sqrt{r^2+z^2}$ is the source-receiver distance, θ is the azimuth , and ϕ is the (south-polar) vertical angle, which satisfies $\cos\phi=-z/R$, $\sin\phi=r/R$, and. In the particular case of unit horizontal and vertical point loads, these stresses are (Note: normal stresses are positive when tensile):

a) Unit horizontal load in x

$$\sigma_r=-\frac{1}{2\pi R^2}\cos\theta\,\sin\phi\left[3\sin^2\phi-\frac{1-2\nu}{\left(1+\cos\phi\right)^2}\right] \tag{A1-1a}$$

$$\sigma_\theta=\frac{1-2\nu}{2\pi R^2}\frac{\cos\theta\left(2+\cos\phi\right)\sin\phi\,\cos\phi}{\left(1+\cos\phi\right)^2} \tag{A1-1b}$$

$$\sigma_z=-\frac{3}{2\pi R^2}\cos\theta\,\sin\phi\,\cos^2\phi \tag{A1-1c}$$

$$\tau_{\theta r}=\tau_{r\theta}=-\frac{1-2\nu}{2\pi R^2}\frac{\sin\theta\,\sin\phi}{\left(1+\cos\phi\right)^2} \tag{A1-1d}$$

$$\tau_{zr}=\tau_{rz}=\frac{3}{2\pi R^2}\cos\theta\,\sin^2\phi\,\cos\phi \tag{A1-1e}$$

$$\tau_{\theta z}=\tau_{z\theta}=0 \tag{A1-1f}$$

b) Unit vertical load in z

$$\sigma_r=\frac{1}{2\pi R^2}\left[3\cos\phi\,\sin^2\phi-\frac{1-2\nu}{1+\cos\phi}\right] \tag{A1-2a}$$

$$\sigma_\theta=\frac{1-2\nu}{2\pi R^2}\left[\frac{1}{1+\cos\phi}-\cos\phi\right] \tag{A1-2b}$$

$$\sigma_z=\frac{3}{2\pi R^2}\cos^3\phi \tag{A1-2c}$$

$$\tau_{zr}=\tau_{rz}=-\frac{3}{2\pi R^2}\sin\phi\,\cos^2\phi \tag{A1-2d}$$

$$\tau_{\theta r}=\tau_{r\theta}=\tau_{\theta z}=\tau_{z\theta}=0 \tag{A1-2e}$$

On the basis of these formulas, the pressure bulbs due to static loads are as listed below. Except as indicated, all bulbs are defined in the vertical $x-z$ plane $(\theta=0)$. Also, ϕ_0 is the angle at which the reference radial distance $R_0=1$ is defined, or more precisely, where the ratio $R/R_0=1$. The angle $\phi_0=0$ defines the vertical axis while $\phi_0=\frac{1}{2}\pi$ is the free surface. Definition of this reference angle facilitates comparisons between static and dynamic results.

a) Unit horizontal load in x

$$\sigma_r: \quad 2(1+\nu)\left(\frac{R}{R_0}\right)^2=\left|3\sin^2\phi-\frac{1-2\nu}{(1+\cos\phi)^2}\right|\sin\phi \qquad \phi_0=\tfrac{1}{2}\pi \qquad \text{(A1-3a)}$$

$$\sigma_\theta: \quad \frac{\left(2+\frac{1}{2}\sqrt{2}\right)}{2\left(1+\frac{1}{2}\sqrt{2}\right)^2}\left(\frac{R}{R_0}\right)^2=\frac{(2+\cos\phi)\sin\phi\cos\phi}{(1+\cos\phi)^2} \qquad \phi_0=\tfrac{1}{4}\pi \qquad \text{(A1-3b)}$$

$$\sigma_z: \quad \left(\tfrac{1}{2}\sqrt{2}\right)^3\left(\frac{R}{R_0}\right)^2=\sin\phi\cos^2\phi \qquad \phi_0=\tfrac{1}{4}\pi \qquad \text{(A1-3c)}$$

$$\tau_{\theta r}: \quad \left(\frac{R}{R_0}\right)^2=\frac{\sin\phi}{(1+\cos\phi)^2} \qquad \text{in } y-z \text{ plane} \qquad \phi_0=\tfrac{1}{2}\pi,\ \theta=90^\circ \qquad \text{(A1-3d)}$$

$$\tau_{zr}: \quad \left(\tfrac{1}{2}\sqrt{2}\right)^3\left(\frac{R}{R_0}\right)^2=\sin^2\phi\cos\phi \qquad \phi_0=\tfrac{1}{4}\pi \qquad \text{(A1-3e)}$$

b) Unit vertical load in z

$$\sigma_r: \quad (1-2\nu)\left(\frac{R}{R_0}\right)^2=\left|3\cos\phi\ \sin^2\phi-\frac{1-2\nu}{1+\cos\phi}\right| \qquad \phi_0=\tfrac{1}{2}\pi \qquad \text{(A1-4a)}$$

$$\sigma_\theta: \quad \left(\frac{R}{R_0}\right)^2=\left|\frac{1}{1+\cos\phi}-\cos\phi\right| \qquad \phi_0=\tfrac{1}{2}\pi \qquad \text{(A1-4b)}$$

$$\sigma_z: \quad \left(\frac{R}{R_0}\right)^2=\cos^3\phi \qquad \phi_0=0 \qquad \text{(A1-4c)}$$

$$\tau_{zr}: \quad \left(\tfrac{1}{2}\sqrt{2}\right)^3\left(\frac{R}{R_0}\right)^2=\sin\phi\cos^2\phi \qquad \phi_0=\tfrac{1}{4}\pi \qquad \text{(A1-4d)}$$

Appendix II: Integral transform for displacements

Consider an elastic half-space $z \le 0$ with mass density ρ, Poisson's ratio ν, shear modulus $\mu = \rho C_S^2$, material (hysteretic) damping ratios ξ_P, ξ_S and wave propagation velocities C_P, C_S for P and S waves, respectively. This half-space is subjected to harmonic horizontal and vertical point loads acting at the surface. The response functions in cylindrical coordinates (with the *z* axis, vertical load and vertical displacement defined positive upwards, see Fig. 1) obtained by integral transform methods are as follows:

a) Horizontal load

$$u_{rx}(r,z,\omega) = \frac{1}{2\pi\mu}\left\{\int_0^\infty f_{xx}\,\frac{d}{d\,kr}J_1(kr)\,dk + \int_0^\infty f_{yy}\,\frac{1}{kr}J_1(kr)\,dk\right\}(\cos\theta) \qquad \text{(A2-1a)}$$

$$u_{\theta x}(r,z,\omega) = \frac{1}{2\pi\mu}\left\{\int_0^\infty f_{xx}\,\frac{1}{kr}J_1(kr)\,dk + \int_0^\infty f_{yy}\,\frac{d}{d\,kr}J_1(kr)\,dk\right\}(-\sin\theta) \qquad \text{(A2-1b)}$$

$$u_{zx}(r,z,\omega) = \frac{1}{2\pi\mu}\left\{\int_0^\infty f_{zx}\,J_1(kr)\,dk\right\}(\cos\theta) \qquad \text{(A2-1c)}$$

b) Vertical load

$$u_{rz}(r,z,\omega) = -\frac{1}{2\pi\mu}\int_0^\infty f_{xz}\,J_1(kr)\,dk \qquad \text{(A2-1d)}$$

$$u_{zz}(r,z,\omega) = \frac{1}{2\pi\mu}\int_0^\infty f_{zz}\,J_0(kr)\,dk \qquad \text{(A2-1e)}$$

The kernels of these expressions involve flexibility functions in the frequency-wavenumber domain $f_{xx}, \cdots f_{zz}$, which are as follows:

$$f_{xx} = \mu k\,G_{xx} = \frac{s}{2\Delta}\left[e_p - \tfrac{1}{2}\left(1+s^2\right)e_s\right] \qquad \text{(A2-2a)}$$

$$f_{zx} = \mu k\,G_{zx} = \frac{1}{2\Delta}\left[ps\,e_p - \tfrac{1}{2}\left(1+s^2\right)e_s\right] \qquad \text{(A2-2b)}$$

$$f_{xz} = \mu k\,G_{xz} = \frac{1}{2\Delta}\left[ps\,e_s - \tfrac{1}{2}\left(1+s^2\right)e_p\right] \qquad \text{(A2-2c)}$$

$$f_{zz} = \mu k\,G_{zz} = \frac{p}{2\Delta}\left[e_s - \tfrac{1}{2}\left(1+s^2\right)e_p\right] \qquad \text{(A2-2d)}$$

$$f_{yy} = \mu k G_{yy} = \frac{1}{s} e_s \qquad \text{(A2-2e)}$$

$$\Delta = ps - \tfrac{1}{4}\left(1 + s^2\right)^2 \qquad \text{= Rayleigh function} \qquad \text{(A2-2f)}$$

in which

$$\frac{1}{C_P^c} = \frac{1 - i\xi_P}{C_P} \qquad \text{complex P-wave velocity} \qquad \text{(A2-3a)}$$

$$\frac{1}{C_S^c} = \frac{1 - i\xi_S}{C_S} \qquad \text{complex S wave velocity} \qquad \text{(A2-3b)}$$

$$p = \sqrt{1 - \left(\frac{\omega}{kC_P^c}\right)^2}, \qquad \mathrm{Im}(p) \geq 0 \qquad \text{(A2-3c)}$$

$$s = \sqrt{1 - \left(\frac{\omega}{kC_S^c}\right)^2}, \qquad \mathrm{Im}(s) \geq 0 \qquad \text{(A2-3d)}$$

$$e_p = \exp(kpz) = \exp(-kp|z|) \qquad \text{(A2-3e)}$$

$$e_s = \exp(ksz) = \exp(-ks|z|) \qquad \text{(A2-3f)}$$

$$a = \frac{C_S}{C_P} = \sqrt{\frac{1 - 2\nu}{2 - 2\nu}} \qquad \text{(A2-3g)}$$

Observe that we use $d = |z|$ as the depth below the surface. We also define the wavenumbers

$$k_P = \frac{\omega}{C_P}, \qquad k_S = \frac{\omega}{C_S}, \qquad k_R = \frac{\omega}{C_R} \qquad \text{(A2-4)}$$

in which C_R is the Rayleigh wave velocity, which satisfies the secular equation $\Delta(k_R) = 0$. The three propagation velocities satisfy the condition $C_R < C_S < C_P$, which implies in turn $k_P < k_S < k_R$. To a close approximation and for any Poisson's ratio, the Rayleigh wave velocity can be obtained as

$$C_R = 0.874 + \left(0.197 - \left(0.056 + 0.0276\nu\right)\nu\right)\nu \qquad \text{(A2-5)}$$

For static loads, the kernels reduce to

$$f_{xx}^0 = \left(1-\nu+\tfrac{1}{2}kz\right)e^{kz}, \qquad f_{xz}^0 = -\tfrac{1}{2}\left(1-2\nu+kz\right)e^{kz} \tag{A2-6a}$$

$$f_{zx}^0 = -\tfrac{1}{2}\left(1-2\nu-kz\right)e^{kz}, \qquad f_{zz}^0 = \left(1-\nu-\tfrac{1}{2}kz\right)e^{kz} \tag{A2-6b}$$

$$f_{yy}^0 = e^{kz} \tag{A2-6c}$$

Observe the changes in sign in kz, which imply $f_{xz}^0 \neq f_{zx}^0$ and $f_{xx}^0 \neq f_{zz}^0$. The numerical integrals are then performed as in equations A2-1a through A2-1d, but replacing f_{ij} by $F_{ij} = f_{ij} - f_{ij}^0$, which effectively subtracts the static solution. This is compensated later by adding explicitly the static solution in the spatial domain, inasmuch as the displacement field for point loads is known.

Similar integral transforms can be written for each and every of the stress components. This requires the availability of the spatial derivatives $\partial u_i / \partial r$ and $\partial u_i / \partial z$, which can be obtained from the above formulas by direct derivation under the integral sign. To avoid mistakes, this is best accomplished via Matlab's symbolic manipulation capabilities, but the final expressions are too complicated to be reproduced herein.

Writing the displacement components for horizontal $(n=1)$ and vertical $(n=0)$ loads as $u_r = \bar{u}_r(r,z)(\cos n\theta)$, $u_\theta = \bar{u}_\theta(r,z)(-\sin n\theta)$ and $u_z = \bar{u}_z(r,z)(\cos n\theta)$, the stresses can be obtained as follows:

a) Circumferential (cylindrical) surfaces

$$\begin{aligned}
\sigma_r &= \left\{(\lambda+2\mu)\frac{\partial \bar{u}_r}{\partial r} + \lambda\left[\frac{\bar{u}_r - n\bar{u}_\theta}{r} + \frac{\partial \bar{u}_z}{\partial z}\right]\right\}(\cos n\theta) \\
\sigma_{\theta r} &= \mu\left\{\frac{\partial \bar{u}_\theta}{\partial r} + \frac{n\bar{u}_r - \bar{u}_\theta}{r}\right\}(-\sin n\theta) \\
\sigma_{zr} &= \mu\left\{\frac{\partial \bar{u}_z}{\partial r} + \frac{\partial \bar{u}_r}{\partial z}\right\}(\cos n\theta)
\end{aligned} \tag{A2-7}$$

b) Radial-vertical surfaces

$$\begin{aligned}
\sigma_{r\theta} &= \mu\left\{\frac{\partial \bar{u}_\theta}{\partial r} + \frac{n\bar{u}_r - \bar{u}_\theta}{r}\right\}(-\sin n\theta) \\
\sigma_\theta &= \left\{\lambda\left[\frac{\partial \bar{u}_r}{\partial r} + \frac{\partial \bar{u}_z}{\partial z}\right] + (\lambda+2\mu)\frac{\bar{u}_r - n\bar{u}_\theta}{r}\right\}(\cos n\theta) \\
\sigma_{z\theta} &= \mu\left\{\frac{\partial \bar{u}_\theta}{\partial z} + \frac{n\bar{u}_z}{r}\right\}(-\sin n\theta)
\end{aligned} \tag{A2-8}$$

c) Horizontal surfaces

$$\sigma_{rz} = \mu\left\{\frac{\partial \bar{u}_z}{\partial r} + \frac{\partial \bar{u}_r}{\partial z}\right\}(\cos n\theta)$$

$$\sigma_{\theta z} = \mu\left\{\frac{n\bar{u}_z}{r} + \frac{\partial \bar{u}_\theta}{\partial z}\right\}(-\sin n\theta) \qquad \text{(A2-9)}$$

$$\sigma_z = \left\{\lambda\left[\frac{\partial \bar{u}_r}{\partial r} + \frac{\bar{u}_r - n\bar{u}_\theta}{r}\right] + (\lambda + 2\mu)\frac{\partial \bar{u}_z}{\partial z}\right\}(\cos n\theta)$$

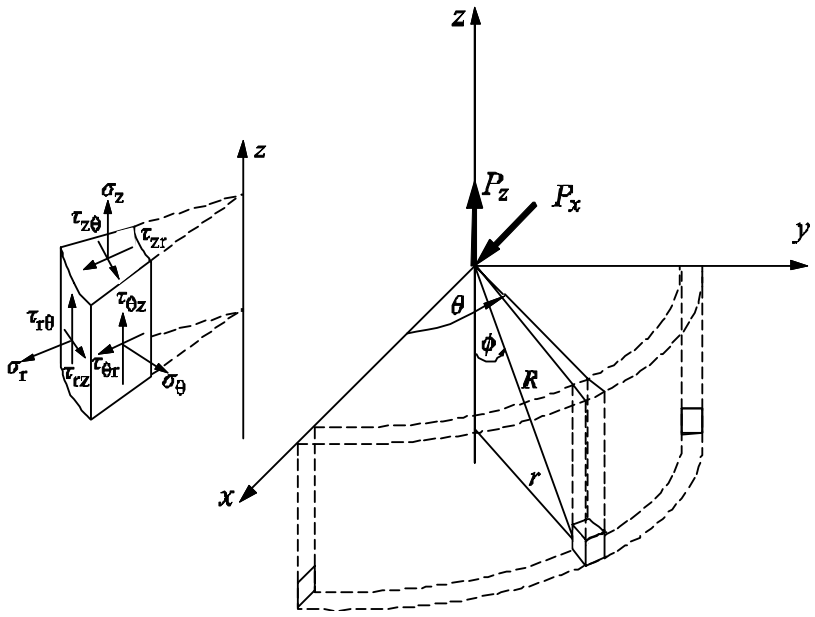

Figure 1: Cartesian vs. spherical coordinates

Horizontal load, ν=0, ξ=0.005, C_S=200 m/s, ρ=1800 kg/m³

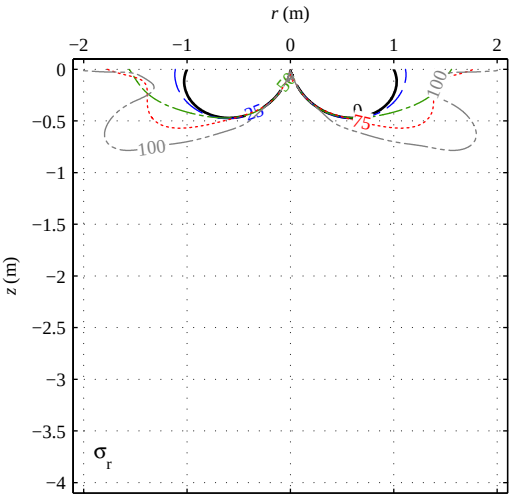

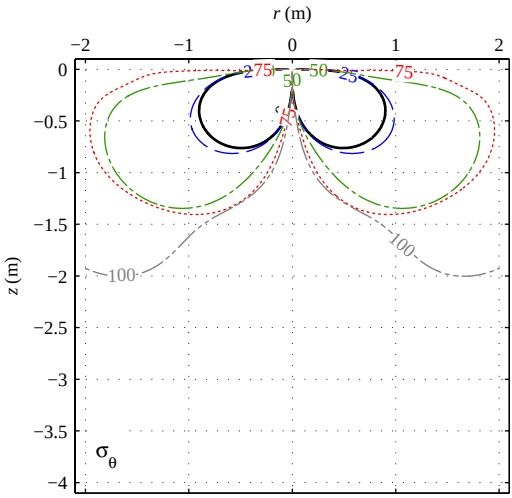

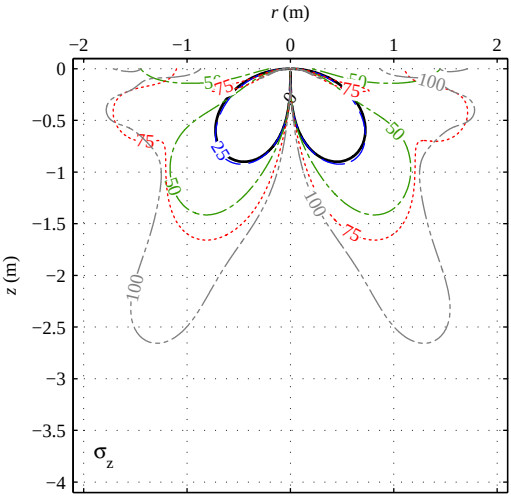

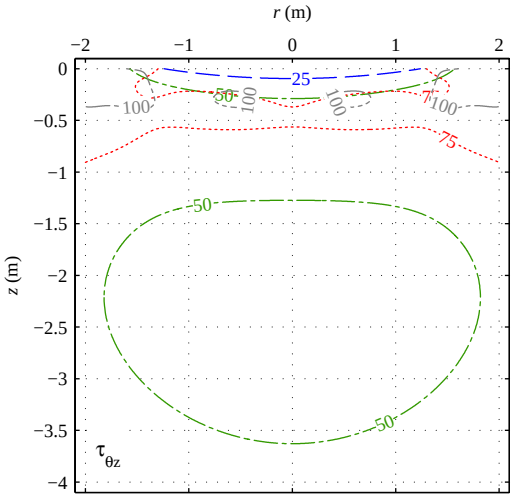

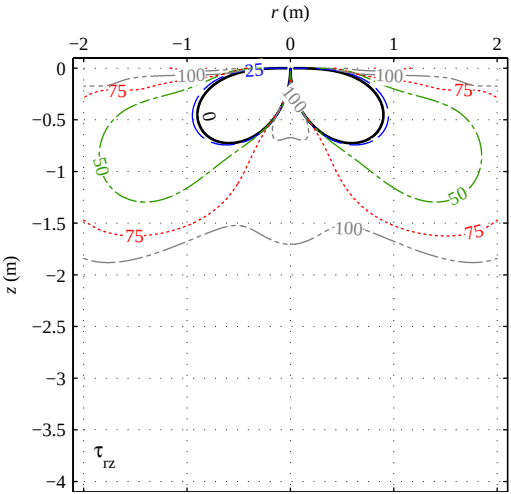

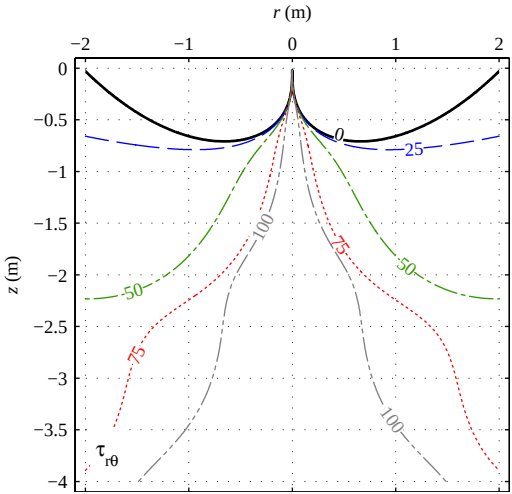

Vertical load, ν=0, ξ=0.005, C_S=200 m/s, ρ=1800 kg/m³

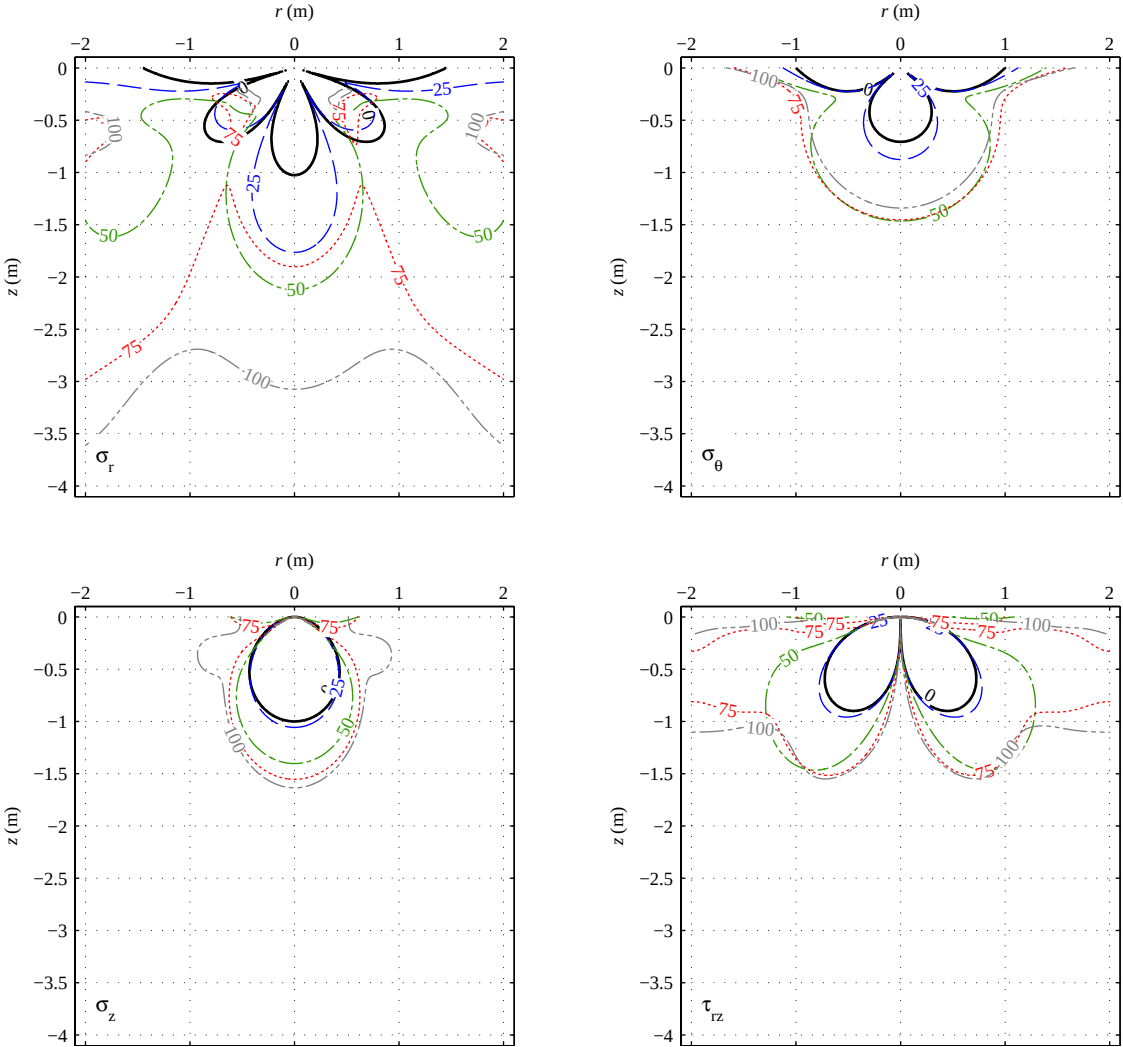

Horizontal load, ν=0.33, ξ=0.005, C_S=200 m/s, ρ=1800 kg/m³

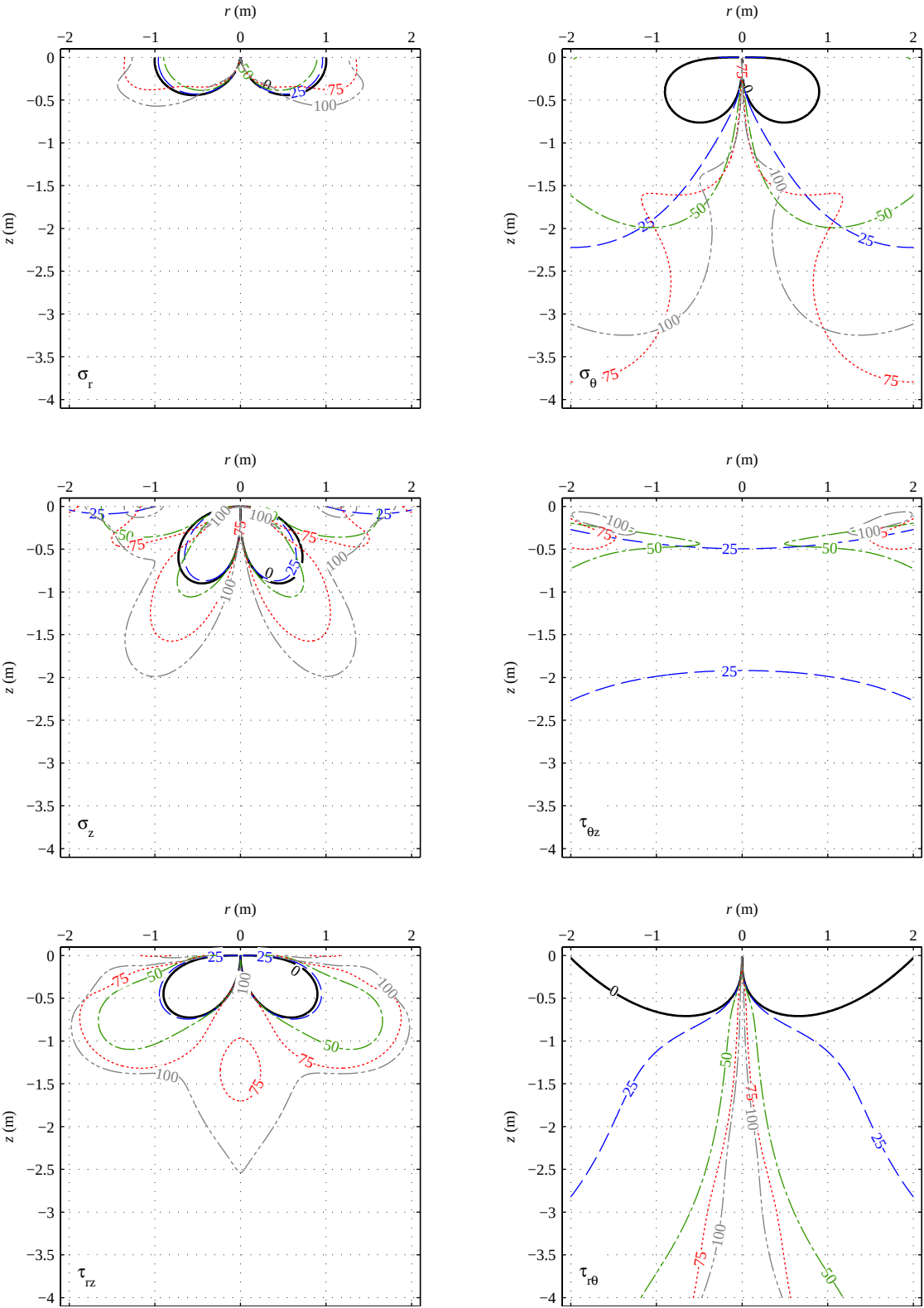

Vertical load, ν=0.33, ξ=0.005, C_S=200 m/s, ρ=1800 kg/m³

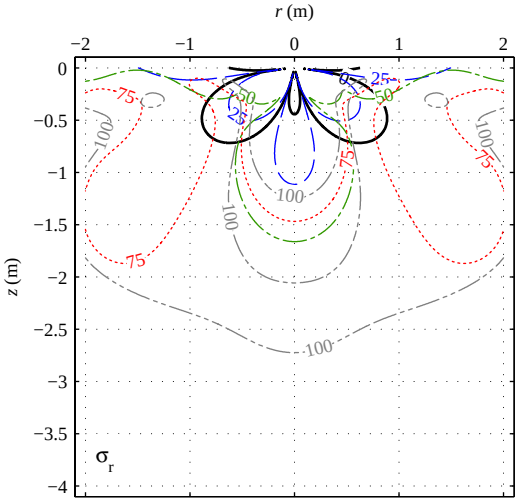

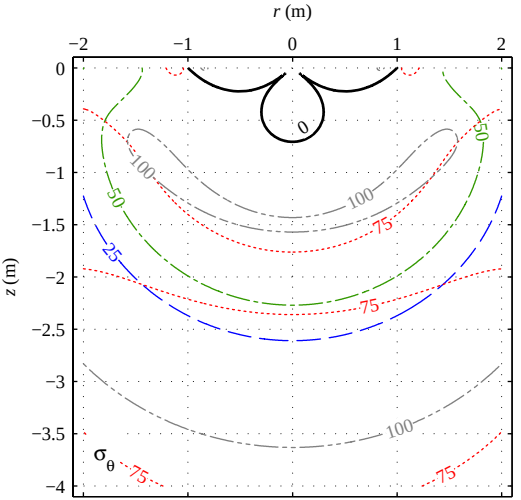

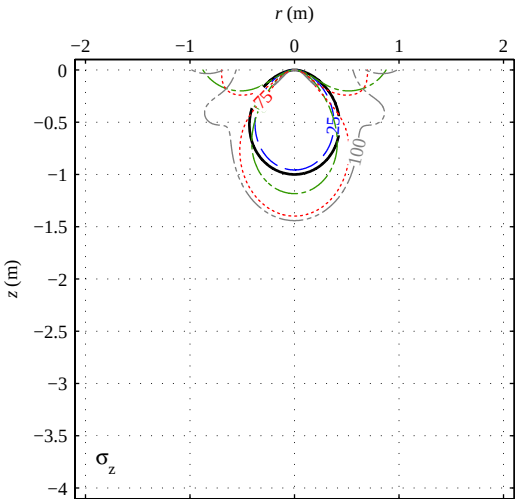

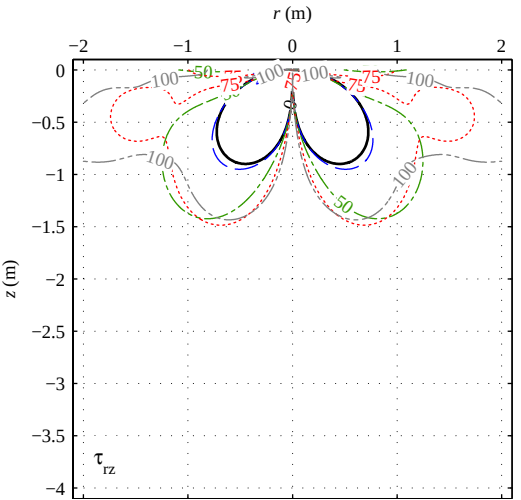

Horizontal load, ν=0.49, ξ=0.005, C_S=200 m/s, ρ=1800 kg/m³

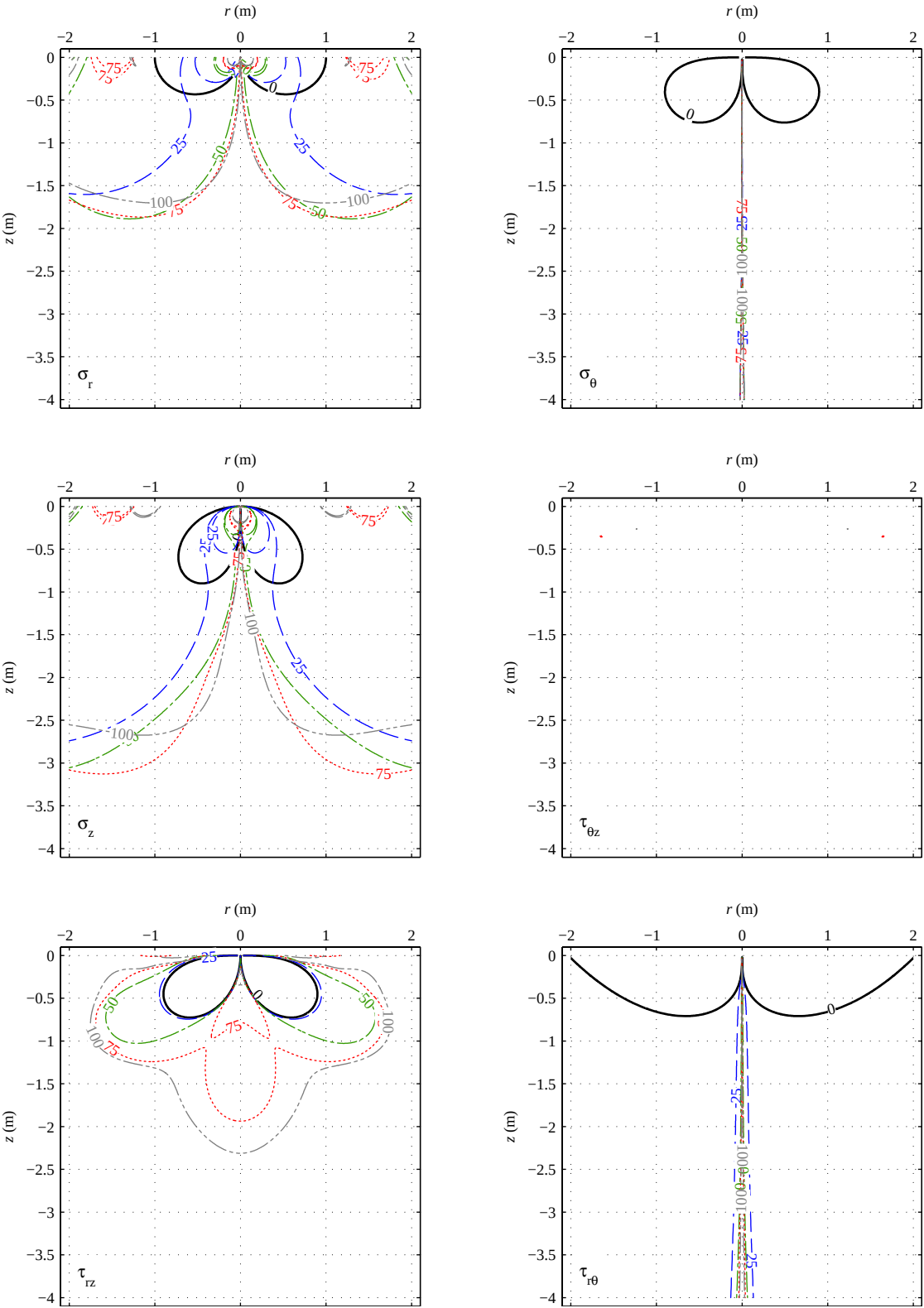

Vertical load, ν=0.49, ξ=0.005, C_S=200 m/s, ρ=1800 kg/m³